

Bounds on an anomalous dijet resonance in $W + \text{jets}$ production in $p\bar{p}$ collisions at $\sqrt{s} = 1.96$ TeV

V.M. Abazov,³⁵ B. Abbott,⁷³ B.S. Acharya,²⁹ M. Adams,⁴⁹ T. Adams,⁴⁷ G.D. Alexeev,³⁵ G. Alkhazov,³⁹
A. Alton^{a, 61} G. Alverson,⁶⁰ G.A. Alves,² M. Aoki,⁴⁸ M. Arov,⁵⁸ A. Askew,⁴⁷ B. Åsman,⁴¹ O. Atramentov,⁶⁵
C. Avila,⁸ J. BackusMayes,⁸⁰ F. Badaud,¹³ L. Bagby,⁴⁸ B. Baldin,⁴⁸ D.V. Bandurin,⁴⁷ S. Banerjee,²⁹ E. Barberis,⁶⁰
P. Baringer,⁵⁶ J. Barreto,³ J.F. Bartlett,⁴⁸ U. Bassler,¹⁸ V. Bazterra,⁴⁹ S. Beale,⁶ A. Bean,⁵⁶ M. Begalli,³
M. Begel,⁷¹ C. Belanger-Champagne,⁴¹ L. Bellantoni,⁴⁸ S.B. Beri,²⁷ G. Bernardi,¹⁷ R. Bernhard,²²
I. Bertram,⁴² M. Besançon,¹⁸ R. Beuselinck,⁴³ V.A. Bezzubov,³⁸ P.C. Bhat,⁴⁸ V. Bhatnagar,²⁷ G. Blazey,⁵⁰
S. Blessing,⁴⁷ K. Bloom,⁶⁴ A. Boehnlein,⁴⁸ D. Boline,⁷⁰ E.E. Boos,³⁷ G. Borissov,⁴² T. Bose,⁵⁹ A. Brandt,⁷⁶
O. Brandt,²³ R. Brock,⁶² G. Brooijmans,⁶⁸ A. Bross,⁴⁸ D. Brown,¹⁷ J. Brown,¹⁷ X.B. Bu,⁴⁸ M. Buehler,⁷⁹
V. Buescher,²⁴ V. Bunichev,³⁷ S. Burdin,^{b, 42} T.H. Burnett,⁸⁰ C.P. Buszello,⁴¹ B. Calpas,¹⁵ E. Camacho-Pérez,³²
M.A. Carrasco-Lizarraga,⁵⁶ B.C.K. Casey,⁴⁸ H. Castilla-Valdez,³² S. Chakrabarti,⁷⁰ D. Chakraborty,⁵⁰
K.M. Chan,⁵⁴ A. Chandra,⁷⁸ G. Chen,⁵⁶ S. Chevalier-Théry,¹⁸ D.K. Cho,⁷⁵ S.W. Cho,³¹ S. Choi,³¹ B. Choudhary,²⁸
S. Cihangir,⁴⁸ D. Claes,⁶⁴ J. Clutter,⁵⁶ M. Cooke,⁴⁸ W.E. Cooper,⁴⁸ M. Corcoran,⁷⁸ F. Couderc,¹⁸
M.-C. Cousinou,¹⁵ A. Croc,¹⁸ D. Cutts,⁷⁵ A. Das,⁴⁵ G. Davies,⁴³ K. De,⁷⁶ S.J. de Jong,³⁴ E. De La Cruz-Burelo,³²
F. Déliot,¹⁸ M. Demarteau,⁴⁸ R. Demina,⁶⁹ D. Denisov,⁴⁸ S.P. Denisov,³⁸ S. Desai,⁴⁸ C. Deterre,¹⁸ K. DeVaughan,⁶⁴
H.T. Diehl,⁴⁸ M. Diesburg,⁴⁸ P.F. Ding,⁴⁴ A. Dominguez,⁶⁴ T. Dorland,⁸⁰ A. Dubey,²⁸ L.V. Dudko,³⁷ D. Duggan,⁶⁵
A. Duperrin,¹⁵ S. Dutt,²⁷ A. Dyshkant,⁵⁰ M. Eads,⁶⁴ D. Edmunds,⁶² J. Ellison,⁴⁶ V.D. Elvira,⁴⁸ Y. Enari,¹⁷
H. Evans,⁵² A. Evdokimov,⁷¹ V.N. Evdokimov,³⁸ G. Facini,⁶⁰ T. Ferbel,⁶⁹ F. Fiedler,²⁴ F. Filthaut,³⁴ W. Fisher,⁶²
H.E. Fisk,⁴⁸ M. Fortner,⁵⁰ H. Fox,⁴² S. Fuess,⁴⁸ A. Garcia-Bellido,⁶⁹ V. Gavrilov,³⁶ P. Gay,¹³ W. Geng,^{15, 62}
D. Gerbaudo,⁶⁶ C.E. Gerber,⁴⁹ Y. Gershtein,⁶⁵ G. Ginther,^{48, 69} G. Golovanov,³⁵ A. Goussiou,⁸⁰ P.D. Grannis,⁷⁰
S. Greder,¹⁹ H. Greenlee,⁴⁸ Z.D. Greenwood,⁵⁸ E.M. Gregores,⁴ G. Grenier,²⁰ Ph. Gris,¹³ J.-F. Grivaz,¹⁶
A. Grohsjean,¹⁸ S. Grünendahl,⁴⁸ M.W. Grünewald,³⁰ T. Guillemín,¹⁶ F. Guo,⁷⁰ G. Gutierrez,⁴⁸ P. Gutierrez,⁷³
A. Haas^{c, 68} S. Hagopian,⁴⁷ J. Haley,⁶⁰ L. Han,⁷ K. Harder,⁴⁴ A. Harel,⁶⁹ J.M. Hauptman,⁵⁵ J. Hays,⁴³ T. Head,⁴⁴
T. Hebbeker,²¹ D. Hedin,⁵⁰ H. Hegab,⁷⁴ A.P. Heinson,⁴⁶ U. Heintz,⁷⁵ C. Hensel,²³ I. Heredia-De La Cruz,³²
K. Herner,⁶¹ G. Hesketh^{d, 44} M.D. Hildreth,⁵⁴ R. Hirosky,⁷⁹ T. Hoang,⁴⁷ J.D. Hobbs,⁷⁰ B. Hoeneisen,¹²
M. Hohlfeld,²⁴ Z. Hubacek,^{10, 18} N. Huske,¹⁷ V. Hynek,¹⁰ I. Iashvili,⁶⁷ Y. Ilchenko,⁷⁷ R. Illingworth,⁴⁸ A.S. Ito,⁴⁸
S. Jabeen,⁷⁵ M. Jaffré,¹⁶ D. Jamin,¹⁵ A. Jayasinghe,⁷³ R. Jesik,⁴³ K. Johns,⁴⁵ M. Johnson,⁴⁸ D. Johnston,⁶⁴
A. Jonckheere,⁴⁸ P. Jonsson,⁴³ J. Joshi,²⁷ A.W. Jung,⁴⁸ A. Juste,⁴⁰ K. Kaadze,⁵⁷ E. Kajfasz,¹⁵ D. Karmanov,³⁷
P.A. Kasper,⁴⁸ I. Katsanos,⁶⁴ R. Kehoe,⁷⁷ S. Kermiche,¹⁵ N. Khalatyan,⁴⁸ A. Khanov,⁷⁴ A. Kharchilava,⁶⁷
Y.N. Kharzheev,³⁵ M.H. Kirby,⁵¹ J.M. Kohli,²⁷ A.V. Kozelov,³⁸ J. Kraus,⁶² S. Kulikov,³⁸ A. Kumar,⁶⁷ A. Kupco,¹¹
T. Kurča,²⁰ V.A. Kuzmin,³⁷ J. Kvita,⁹ S. Lammers,⁵² G. Landsberg,⁷⁵ P. Lebrun,²⁰ H.S. Lee,³¹ S.W. Lee,⁵⁵
W.M. Lee,⁴⁸ J. Lellouch,¹⁷ L. Li,⁴⁶ Q.Z. Li,⁴⁸ S.M. Lietti,⁵ J.K. Lim,³¹ D. Lincoln,⁴⁸ J. Linnemann,⁶²
V.V. Lipaev,³⁸ R. Lipton,⁴⁸ Y. Liu,⁷ Z. Liu,⁶ A. Lobodenko,³⁹ M. Lokajicek,¹¹ R. Lopes de Sa,⁷⁰ H.J. Lubatti,⁸⁰
R. Luna-Garcia^{e, 32} A.L. Lyon,⁴⁸ A.K.A. Maciel,² D. Mackin,⁷⁸ R. Madar,¹⁸ R. Magaña-Villalba,³² S. Malik,⁶⁴
V.L. Malyshev,³⁵ Y. Maravin,⁵⁷ J. Martínez-Ortega,³² R. McCarthy,⁷⁰ C.L. McGivern,⁵⁶ M.M. Meijer,³⁴
A. Melnitchouk,⁶³ D. Menezes,⁵⁰ P.G. Mercadante,⁴ M. Merkin,³⁷ A. Meyer,²¹ J. Meyer,²³ F. Miconi,¹⁹
N.K. Mondal,²⁹ G.S. Muanza,¹⁵ M. Mulhearn,⁷⁹ E. Nagy,¹⁵ M. Naimuddin,²⁸ M. Narain,⁷⁵ R. Nayyar,²⁸
H.A. Neal,⁶¹ J.P. Negret,⁸ P. Neustroev,³⁹ S.F. Novaes,⁵ T. Nunnemann,²⁵ G. Obrant^{†, 39} J. Orduna,⁷⁸ N. Osman,¹⁵
J. Osta,⁵⁴ G.J. Otero y Garzón,¹ M. Padilla,⁴⁶ A. Pal,⁷⁶ N. Parashar,⁵³ V. Parihar,⁷⁵ S.K. Park,³¹ J. Parsons,⁶⁸
R. Partridge^{c, 75} N. Parua,⁵² A. Patwa,⁷¹ B. Penning,⁴⁸ M. Perfilov,³⁷ K. Peters,⁴⁴ Y. Peters,⁴⁴ K. Petridis,⁴⁴
G. Petrillo,⁶⁹ P. Pétroff,¹⁶ R. Piegaia,¹ M.-A. Pleier,⁷¹ P.L.M. Podesta-Lerma^{f, 32} V.M. Podstavkov,⁴⁸ P. Polozov,³⁶
A.V. Popov,³⁸ M. Prewitt,⁷⁸ D. Price,⁵² N. Prokopenko,³⁸ S. Protopopescu,⁷¹ J. Qian,⁶¹ A. Quadt,²³ B. Quinn,⁶³
M.S. Rangel,² K. Ranjan,²⁸ P.N. Ratoff,⁴² I. Razumov,³⁸ P. Renkel,⁷⁷ M. Rijssenbeek,⁷⁰ I. Ripp-Baudot,¹⁹
F. Rizatdinova,⁷⁴ M. Rominsky,⁴⁸ A. Ross,⁴² C. Royon,¹⁸ P. Rubinov,⁴⁸ R. Ruchti,⁵⁴ G. Safronov,³⁶ G. Sajot,¹⁴
P. Salcido,⁵⁰ A. Sánchez-Hernández,³² M.P. Sanders,²⁵ B. Sanghi,⁴⁸ A.S. Santos,⁵ G. Savage,⁴⁸ L. Sawyer,⁵⁸
T. Scanlon,⁴³ R.D. Schamberger,⁷⁰ Y. Scheglov,³⁹ H. Schellman,⁵¹ T. Schliephake,²⁶ S. Schlobohm,⁸⁰

C. Schwanenberger,⁴⁴ R. Schwienhorst,⁶² J. Sekaric,⁵⁶ H. Severini,⁷³ E. Shabalina,²³ V. Shary,¹⁸ A.A. Shchukin,³⁸ R.K. Shivpuri,²⁸ V. Simak,¹⁰ V. Sirotenko,⁴⁸ P. Skubic,⁷³ P. Slattery,⁶⁹ D. Smirnov,⁵⁴ K.J. Smith,⁶⁷ G.R. Snow,⁶⁴ J. Snow,⁷² S. Snyder,⁷¹ S. Söldner-Rembold,⁴⁴ L. Sonnenschein,²¹ K. Soustruznik,⁹ J. Stark,¹⁴ V. Stolin,³⁶ D.A. Stoyanova,³⁸ M. Strauss,⁷³ D. Strom,⁴⁹ L. Stutte,⁴⁸ L. Suter,⁴⁴ P. Svoisky,⁷³ M. Takahashi,⁴⁴ A. Tanasijczuk,¹ W. Taylor,⁶ M. Titov,¹⁸ V.V. Tokmenin,³⁵ Y.-T. Tsai,⁶⁹ D. Tsybychev,⁷⁰ B. Tuchming,¹⁸ C. Tully,⁶⁶ L. Uvarov,³⁹ S. Uvarov,³⁹ S. Uzunyan,⁵⁰ R. Van Kooten,⁵² W.M. van Leeuwen,³³ N. Varelas,⁴⁹ E.W. Varnes,⁴⁵ I.A. Vasilyev,³⁸ P. Verdier,²⁰ L.S. Vertogradov,³⁵ M. Verzocchi,⁴⁸ M. Vesterinen,⁴⁴ D. Vilanova,¹⁸ P. Vokac,¹⁰ H.D. Wahl,⁴⁷ M.H.L.S. Wang,⁴⁸ J. Warchol,⁵⁴ G. Watts,⁸⁰ M. Wayne,⁵⁴ M. Weber,^{9, 48} L. Welty-Rieger,⁵¹ A. White,⁷⁶ D. Wicke,²⁶ M.R.J. Williams,⁴² G.W. Wilson,⁵⁶ M. Wobisch,⁵⁸ D.R. Wood,⁶⁰ T.R. Wyatt,⁴⁴ Y. Xie,⁴⁸ C. Xu,⁶¹ S. Yacoob,⁵¹ R. Yamada,⁴⁸ W.-C. Yang,⁴⁴ T. Yasuda,⁴⁸ Y.A. Yatsunenko,³⁵ Z. Ye,⁴⁸ H. Yin,⁴⁸ K. Yip,⁷¹ S.W. Youn,⁴⁸ J. Yu,⁷⁶ S. Zelitch,⁷⁹ T. Zhao,⁸⁰ B. Zhou,⁶¹ J. Zhu,⁶¹ M. Zielinski,⁶⁹ D. Zieminska,⁵² and L. Zivkovic⁷⁵

(The D0 Collaboration*)

¹Universidad de Buenos Aires, Buenos Aires, Argentina

²LAFEX, Centro Brasileiro de Pesquisas Físicas, Rio de Janeiro, Brazil

³Universidade do Estado do Rio de Janeiro, Rio de Janeiro, Brazil

⁴Universidade Federal do ABC, Santo André, Brazil

⁵Instituto de Física Teórica, Universidade Estadual Paulista, São Paulo, Brazil

⁶Simon Fraser University, Vancouver, British Columbia, and York University, Toronto, Ontario, Canada

⁷University of Science and Technology of China, Hefei, People's Republic of China

⁸Universidad de los Andes, Bogotá, Colombia

⁹Charles University, Faculty of Mathematics and Physics,
Center for Particle Physics, Prague, Czech Republic

¹⁰Czech Technical University in Prague, Prague, Czech Republic

¹¹Center for Particle Physics, Institute of Physics,
Academy of Sciences of the Czech Republic, Prague, Czech Republic

¹²Universidad San Francisco de Quito, Quito, Ecuador

¹³LPC, Université Blaise Pascal, CNRS/IN2P3, Clermont, France

¹⁴LPSC, Université Joseph Fourier Grenoble 1, CNRS/IN2P3,
Institut National Polytechnique de Grenoble, Grenoble, France

¹⁵CPPM, Aix-Marseille Université, CNRS/IN2P3, Marseille, France

¹⁶LAL, Université Paris-Sud, CNRS/IN2P3, Orsay, France

¹⁷LPNHE, Universités Paris VI and VII, CNRS/IN2P3, Paris, France

¹⁸CEA, Irfu, SPP, Saclay, France

¹⁹IPHC, Université de Strasbourg, CNRS/IN2P3, Strasbourg, France

²⁰IPNL, Université Lyon 1, CNRS/IN2P3, Villeurbanne, France and Université de Lyon, Lyon, France

²¹III. Physikalisches Institut A, RWTH Aachen University, Aachen, Germany

²²Physikalisches Institut, Universität Freiburg, Freiburg, Germany

²³II. Physikalisches Institut, Georg-August-Universität Göttingen, Göttingen, Germany

²⁴Institut für Physik, Universität Mainz, Mainz, Germany

²⁵Ludwig-Maximilians-Universität München, München, Germany

²⁶Fachbereich Physik, Bergische Universität Wuppertal, Wuppertal, Germany

²⁷Panjab University, Chandigarh, India

²⁸Delhi University, Delhi, India

²⁹Tata Institute of Fundamental Research, Mumbai, India

³⁰University College Dublin, Dublin, Ireland

³¹Korea Detector Laboratory, Korea University, Seoul, Korea

³²CINVESTAV, Mexico City, Mexico

³³Nikhef, Science Park, Amsterdam, the Netherlands

³⁴Radboud University Nijmegen, Nijmegen, the Netherlands and Nikhef, Science Park, Amsterdam, the Netherlands

³⁵Joint Institute for Nuclear Research, Dubna, Russia

³⁶Institute for Theoretical and Experimental Physics, Moscow, Russia

³⁷Moscow State University, Moscow, Russia

³⁸Institute for High Energy Physics, Protvino, Russia

³⁹Petersburg Nuclear Physics Institute, St. Petersburg, Russia

⁴⁰Institució Catalana de Recerca i Estudis Avançats (ICREA) and Institut de Física d'Altes Energies (IFAE), Barcelona, Spain

⁴¹Stockholm University, Stockholm and Uppsala University, Uppsala, Sweden

⁴²Lancaster University, Lancaster LA1 4YB, United Kingdom

⁴³Imperial College London, London SW7 2AZ, United Kingdom

⁴⁴The University of Manchester, Manchester M13 9PL, United Kingdom

⁴⁵University of Arizona, Tucson, Arizona 85721, USA

- ⁴⁶University of California Riverside, Riverside, California 92521, USA
⁴⁷Florida State University, Tallahassee, Florida 32306, USA
⁴⁸Fermi National Accelerator Laboratory, Batavia, Illinois 60510, USA
⁴⁹University of Illinois at Chicago, Chicago, Illinois 60607, USA
⁵⁰Northern Illinois University, DeKalb, Illinois 60115, USA
⁵¹Northwestern University, Evanston, Illinois 60208, USA
⁵²Indiana University, Bloomington, Indiana 47405, USA
⁵³Purdue University Calumet, Hammond, Indiana 46323, USA
⁵⁴University of Notre Dame, Notre Dame, Indiana 46556, USA
⁵⁵Iowa State University, Ames, Iowa 50011, USA
⁵⁶University of Kansas, Lawrence, Kansas 66045, USA
⁵⁷Kansas State University, Manhattan, Kansas 66506, USA
⁵⁸Louisiana Tech University, Ruston, Louisiana 71272, USA
⁵⁹Boston University, Boston, Massachusetts 02215, USA
⁶⁰Northeastern University, Boston, Massachusetts 02115, USA
⁶¹University of Michigan, Ann Arbor, Michigan 48109, USA
⁶²Michigan State University, East Lansing, Michigan 48824, USA
⁶³University of Mississippi, University, Mississippi 38677, USA
⁶⁴University of Nebraska, Lincoln, Nebraska 68588, USA
⁶⁵Rutgers University, Piscataway, New Jersey 08855, USA
⁶⁶Princeton University, Princeton, New Jersey 08544, USA
⁶⁷State University of New York, Buffalo, New York 14260, USA
⁶⁸Columbia University, New York, New York 10027, USA
⁶⁹University of Rochester, Rochester, New York 14627, USA
⁷⁰State University of New York, Stony Brook, New York 11794, USA
⁷¹Brookhaven National Laboratory, Upton, New York 11973, USA
⁷²Langston University, Langston, Oklahoma 73050, USA
⁷³University of Oklahoma, Norman, Oklahoma 73019, USA
⁷⁴Oklahoma State University, Stillwater, Oklahoma 74078, USA
⁷⁵Brown University, Providence, Rhode Island 02912, USA
⁷⁶University of Texas, Arlington, Texas 76019, USA
⁷⁷Southern Methodist University, Dallas, Texas 75275, USA
⁷⁸Rice University, Houston, Texas 77005, USA
⁷⁹University of Virginia, Charlottesville, Virginia 22901, USA
⁸⁰University of Washington, Seattle, Washington 98195, USA
(Dated: June 9, 2011)

We present a study of the dijet invariant mass spectrum in events with two jets produced in association with a W boson in data corresponding to an integrated luminosity of 4.3 fb^{-1} collected with the D0 detector at $\sqrt{s} = 1.96 \text{ TeV}$. We find no evidence for anomalous resonant dijet production and derive upper limits on the production cross section of an anomalous dijet resonance recently reported by the CDF Collaboration, investigating the range of dijet invariant mass from 110 to $170 \text{ GeV}/c^2$. The probability of the D0 data being consistent with the presence of a dijet resonance with 4 pb production cross section at $145 \text{ GeV}/c^2$ is 8×10^{-6} .

PACS numbers: 12.15.Ji, 12.38.Qk, 13.85.Rm, 14.80.-j

The CDF Collaboration at the Fermilab Tevatron $p\bar{p}$ collider recently reported a study of the dijet invariant mass (M_{jj}) spectrum in associated production with $W \rightarrow \ell\nu$ ($\ell = e$ or μ) at $\sqrt{s} = 1.96 \text{ TeV}$ with an integrated luminosity of 4.3 fb^{-1} [1]. In that paper they present evidence for an excess of events corresponding to

3.2 standard deviations (s.d.) above the background expectation, centered at $M_{jj} = 144 \pm 5 \text{ GeV}/c^2$ [1]. The CDF authors model this excess using a Gaussian peak with a width corresponding to an expected experimental M_{jj} resolution for the CDF detector [2] of $14.3 \text{ GeV}/c^2$ and further estimate the acceptance and selection efficiencies by simulating associated W + Higgs boson (H) production in the decay mode $H \rightarrow b\bar{b}$ and with a mass $M_H = 150 \text{ GeV}/c^2$. Assuming the excess is caused by a particle X with $\mathcal{B}(X \rightarrow jj) = 1$, the CDF Collaboration reports an estimated production cross section of $\sigma(p\bar{p} \rightarrow WX) \approx 4 \text{ pb}$.

Using 5.3 fb^{-1} of integrated luminosity, the D0 Collaboration has previously set limits on resonant $b\bar{b}$ pro-

*with visitors from ^aAugustana College, Sioux Falls, SD, USA, ^bThe University of Liverpool, Liverpool, UK, ^cSLAC, Menlo Park, CA, USA, ^dUniversity College London, London, UK, ^eCentro de Investigacion en Computacion - IPN, Mexico City, Mexico, ^fECFM, Universidad Autonoma de Sinaloa, Culiacán, Mexico, and ^gUniversität Bern, Bern, Switzerland. [‡]Deceased.

duction in association with a W boson in dedicated searches for standard model (SM) Higgs bosons in the $WH \rightarrow \ell\nu b\bar{b}$ channel [3]. The D0 Collaboration reported upper limits on $\sigma(p\bar{p} \rightarrow WH) \times \mathcal{B}(H \rightarrow b\bar{b})$ ranging from approximately 0.62 pb for $M_H = 100 \text{ GeV}/c^2$ to 0.33 pb for $M_H = 150 \text{ GeV}/c^2$. The CDF Collaboration has performed a similar search using 2.7 fb^{-1} of integrated luminosity and reported no excess of events [4]. Furthermore, the D0 Collaboration has not observed a significant excess of associated W boson and dijet production in analyses of either $WW/WZ \rightarrow \ell\nu jj$ [5] or $H \rightarrow WW \rightarrow \ell\nu jj$ [6] using 1.1 fb^{-1} and 5.4 fb^{-1} of integrated luminosity, respectively.

In this Letter we report a study of associated $W(\rightarrow \ell\nu)$ and dijet production using data corresponding to 4.3 fb^{-1} of integrated luminosity collected with the D0 detector [7] at $\sqrt{s} = 1.96 \text{ TeV}$ at the Fermilab Tevatron $p\bar{p}$ Collider. The CDF study of this production process uses the same integrated luminosity. We investigate the dijet invariant mass range from 110 to $170 \text{ GeV}/c^2$ for evidence of anomalous dijet production.

To select $W(\rightarrow \ell\nu) + jj$ candidate events, we impose similar selection criteria to those used in the CDF analysis: a single reconstructed lepton (electron or muon) with transverse momentum $p_T > 20 \text{ GeV}/c$ and pseudorapidity [8] $|\eta| < 1.0$; missing transverse energy $\cancel{E}_T > 25 \text{ GeV}$; two jets reconstructed using a jet cone algorithm [9] with a cone of radius $\Delta\mathcal{R} = 0.5$ that satisfy $p_T > 30 \text{ GeV}/c$ and $|\eta| < 2.5$, while vetoing events with additional jets with $p_T > 30 \text{ GeV}/c$. The separation between the two jets must be $|\Delta\eta(\text{jet}_1, \text{jet}_2)| < 2.5$, and the azimuthal separation between the most energetic jet and the direction of the \cancel{E}_T must satisfy $\Delta\phi(\text{jet}, \cancel{E}_T) > 0.4$. The transverse momentum of the dijet system is required to be $p_T(jj) > 40 \text{ GeV}/c$. To reduce the background from processes that do not contain $W \rightarrow \ell\nu$ decays, we require a transverse mass [10] of $M_T^{\ell\nu} > 30 \text{ GeV}/c^2$. In addition, we restrict $M_T^{\mu\nu} < 200 \text{ GeV}/c^2$ to suppress muon candidates with poorly measured momenta. Candidate events in the electron channel are required to satisfy a single electron trigger or a trigger requiring electrons and jets, which results in a combined trigger efficiency for the $e\nu jj$ selection of $(98^{+2}_{-3})\%$. A suite of triggers in the muon channel achieves a trigger efficiency of $(95 \pm 5)\%$ for the $\mu\nu jj$ selection. Lepton candidates must be spatially matched to a track that originates from the $p\bar{p}$ interaction vertex and they must be isolated from other energy depositions in the calorimeter and other tracks in the central tracking detector.

Most background processes are modeled using Monte Carlo (MC) simulation as in the CDF analysis. Diboson contributions (WW , WZ , ZZ) are generated with PYTHIA [11] using CTEQ6L1 parton distribution functions (PDF) [12]. The fixed-order matrix element (FOME) generator ALPGEN [13] with CTEQ6L1 PDF is used to generate W +jets, Z +jets, and $t\bar{t}$ events. The

FOME generator COMPHEP [14] is used to produce single top-quark MC samples with CTEQ6M PDF. Both ALPGEN and COMPHEP are interfaced to PYTHIA for subsequent parton showering and hadronization. The MC events undergo a GEANT-based [15] detector simulation and are reconstructed using the same algorithms as used for D0 data. The effect of multiple $p\bar{p}$ interactions is included by overlaying data events from random beam crossings on simulated events. All MC samples except the W +jets are normalized to next-to-leading order (NLO) or next-to-NLO (NNLO) predictions for SM cross sections; the $t\bar{t}$, single t , and diboson cross sections are taken from Ref. [16], Ref. [17], and the MCFM program [18], respectively. The Z +jets sample is normalized to the NNLO cross section [19]. The multijet background, in which a jet misidentified as an isolated lepton passes all selection requirements, is determined from data. In the muon channel, the multijet background is modeled with data events that fail the muon isolation requirements, but pass all other selections. In the electron channel, the multijet background is estimated using a data sample containing events that pass loosened electron quality requirements, but fail the tight electron quality criteria. All multijet samples are corrected for contributions from processes modeled by MC. The multijet normalizations in the two lepton channels are determined from fits to the $M_T^{\ell\nu}$ distributions, in which the multijet and W +jets relative normalizations are allowed to float. The expected rate of multijet background is determined by this normalization, with an assigned uncertainty of 20%.

Corrections are applied to the MC to account for differences from data in reconstruction and identification efficiencies of leptons and jets. Also, trigger efficiencies measured in data are applied to MC. The instantaneous luminosity profile and z position of the $p\bar{p}$ interaction vertex of each MC sample are adjusted to match those in data. The p_T distribution of Z bosons is corrected at the generator level to reproduce dedicated measurements [20].

Other D0 analyses of this final state apply additional corrections to improve the modeling of the W +jets and Z +jets production in the MC [3]. For the results presented in this Letter, we choose not to apply those corrections in order to parallel the CDF analysis. We did, however, study the effects of applying such corrections [21] and find they do not alter our conclusions.

We consider the effect of systematic uncertainties on both the normalization and the shape of dijet invariant mass distributions. Systematic effects are considered from a range of sources: the choice of renormalization and factorization scales, the ALPGEN parton-jet matching algorithm [22], jet energy resolution, jet energy scale, and modeling of the underlying event and parton showering. Uncertainties on the choice of PDF, as well as uncertainties from object reconstruction and identification, are evaluated for all MC samples.

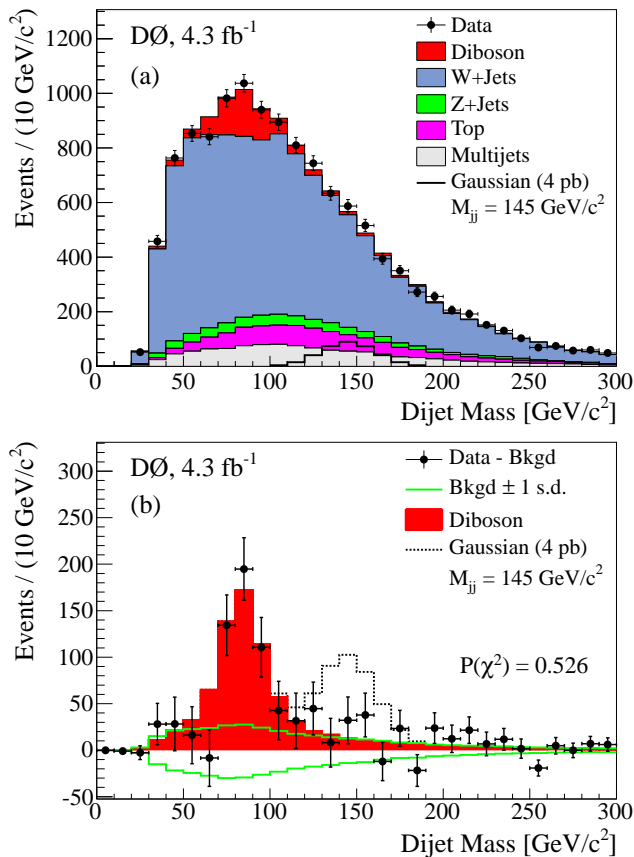


FIG. 1: (color online) Dijet invariant mass summed over electron and muon channels after the fit without (a) and with (b) subtraction of SM contributions other than that from the SM diboson processes, along with the ± 1 s.d. systematic uncertainty on all SM predictions. The χ^2 fit probability, $P(\chi^2)$, is based on the residuals using data and MC statistical uncertainties. Also shown is the relative size and shape for a model with a Gaussian resonance with a production cross section of 4 pb at $M_{jj} = 145$ GeV/c².

In Fig. 1 we present the dijet invariant mass distribution after a fit of the sum of SM contributions to data. Other distributions are available in the supplementary material [21]. The fit minimizes a Poisson χ^2 -function with respect to variations in the rates of individual background sources and systematic uncertainties that may modify the predicted dijet invariant mass distribution [23]. A Gaussian prior is used for each systematic uncertainty, including those on the normalization of each sample, but the cross sections for diboson and W+jets production in the MC are floated with no constraint. The fit computes the optimal values of the systematic uncertainties, accounting for departures from the nominal predictions by including a term in the fit function that sums the squared deviation of each systematic in units normalized by its ± 1 s.d. Different uncertainties are assumed to be mutually independent, but those common to both lepton channels are treated as fully correlated. We per-

TABLE I: Yields determined following a χ^2 fit to the data, as shown in Fig. 1. The total uncertainty includes the effect of correlations between the individual contributions as determined using the covariance matrix.

	Electron channel	Muon channel
Dibosons	434 ± 38	304 ± 25
W+jets	5620 ± 500	3850 ± 290
Z+jets	180 ± 42	350 ± 60
$t\bar{t}$ + single top	600 ± 69	363 ± 39
Multijet	932 ± 230	151 ± 69
Total predicted	7770 ± 170	5020 ± 130
Data	7763	5026

form fits to electron and muon selections simultaneously and then sum them to obtain the dijet invariant mass distributions shown in Fig. 1. The measured yields after the fit are given in Table I.

To probe for an excess similar to that observed by the CDF Collaboration [1], we model a possible signal as a Gaussian resonance in the dijet invariant mass with an observed width corresponding to the expected resolution of the D0 detector given by $\sigma_{jj} = \sigma_{W \rightarrow jj} \cdot \sqrt{M_{jj}/M_{W \rightarrow jj}}$. Here, $\sigma_{W \rightarrow jj}$ and $M_{W \rightarrow jj}$ are the width and mass of the $W \rightarrow jj$ resonance, determined to be $\sigma_{W \rightarrow jj} = 11.7$ GeV/c² and $M_{W \rightarrow jj} = 81$ GeV/c² from a simulation of $WW \rightarrow \ell\nu jj$ production. For a dijet invariant mass resonance at $M_{jj} = 145$ GeV/c², the expected width is $\sigma_{jj} = 15.7$ GeV/c².

We normalize the Gaussian model in the same way as reported in the CDF Letter [1]. We assume that any such excess comes from a particle X that decays to jets with 100% branching fraction. The acceptance for this hypothetical process ($WX \rightarrow \ell\nu jj$) is estimated from a MC simulation of $WH \rightarrow \ell\nu b\bar{b}$ production. When testing the Gaussian signal with a mean of $M_{jj} = 145$ GeV/c², the acceptance is taken from the $WH \rightarrow \ell\nu b\bar{b}$ simulation with $M_H = 150$ GeV/c². This prescription is chosen to be consistent with the CDF analysis, which used a simulation of $WH \rightarrow \ell\nu b\bar{b}$ production with $M_H = 150$ GeV/c² to estimate the acceptance for the excess that they observe at $M_{jj} = 144$ GeV/c². When probing other values of M_{jj} , we use the acceptance obtained for $WH \rightarrow \ell\nu b\bar{b}$ MC events with $M_H = M_{jj} + 5$ GeV/c².

We use this Gaussian model to derive upper limits on the cross section for a possible dijet resonance as a function of dijet invariant mass using the CL_s method with a negative log-likelihood ratio (LLR) test statistic [24] that is summed over all bins in the dijet invariant mass spectrum. Upper limits on cross section are calculated at the 95% confidence level (C.L.) for Gaussian signals with mean dijet invariant mass in the range $110 < M_{jj} < 170$ GeV/c², in steps of 5 GeV/c², allowing the cross sections for W+jets production to float with no constraint. Other contributions are constrained by the *a priori* uncertainties on their rate, either derived from

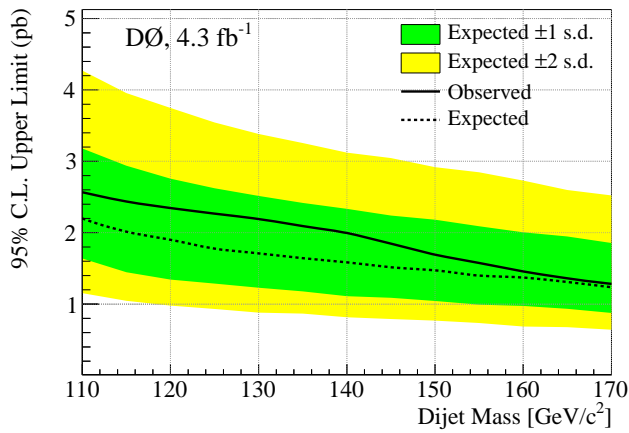


FIG. 2: (color online) Upper limits on the cross section (in pb) at the 95% C.L. for a Gaussian signal in dijet invariant mass. Shown are the limit expected using the background prediction, the observed data, and the regions corresponding to a 1 s.d. and 2 s.d. fluctuation of the backgrounds.

theory or subsidiary measurements.

The Gaussian model is assigned systematic uncertainties affecting both the normalization and shape of the distribution derived from the systematic uncertainties on the diboson simulation. A fit [23] of both the signal+background and background-only hypotheses is performed for an ensemble of pseudo-experiments as well as for the data distribution. The results of the cross section upper limit calculation are shown in Fig. 2 and are summarized in Table II.

In a further effort to evaluate the sensitivity for any excess of events of the type reported by the CDF Collaboration, we perform a signal-injection test. We repeat the statistical analysis after injecting a Gaussian signal model, normalized to a cross section of 4 pb, into the D0 data sample, thereby creating a mock “data” sample modeling the expected outcome with a signal present. The size and shape of the injected Gaussian model for $M_{jj} = 145 \text{ GeV}/c^2$ relative to other data components is shown in Fig. 1.

The LLR metric provides a sensitive measure of model compatibility, providing information on both the rate and mass of any signal-like excess. We therefore study the LLR distributions obtained with actual data as well as the signal-injected mock data sample. The results of the LLR test in Fig. 3 show a striking difference between the two hypotheses, demonstrating that this analysis is sensitive to the purported excess. In the actual data, however, no significant evidence for an excess is observed.

In Fig. 4, we show as a function of cross section the p -value obtained by integrating the LLR distribution populated from pseudo-experiments drawn from the signal+background hypothesis above the observed LLR, assuming a Gaussian invariant mass distribution with a mean of $M_{jj} = 145 \text{ GeV}/c^2$. The p -value for a Gaussian

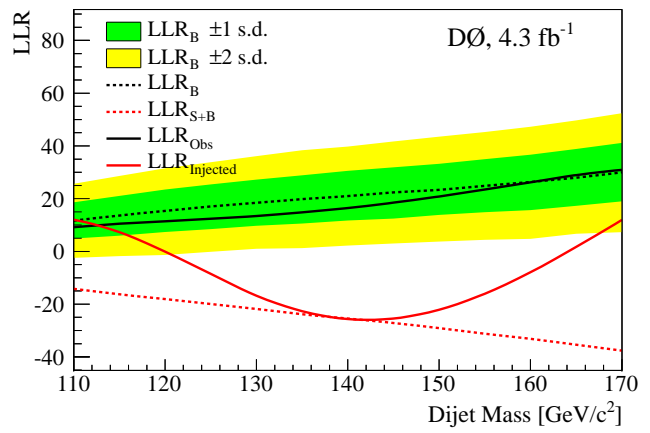


FIG. 3: (color online) Log-likelihood ratio test statistic as a function of probed dijet mass. Shown are the expected LLR for the background prediction (dashed black) with regions corresponding to a 1 s.d. and 2 s.d. fluctuation of the backgrounds, for the signal+background prediction (dashed red), for the observed data (solid black), and for data with a dijet invariant mass resonance at $145 \text{ GeV}/c^2$ injected with a cross section of 4 pb (solid red).

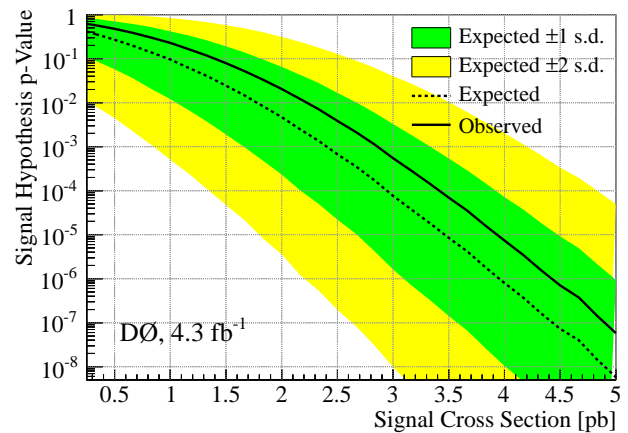


FIG. 4: (color online) Distribution of p -values for the signal+background hypothesis with a Gaussian signal with mean of $M_{jj} = 145 \text{ GeV}/c^2$ as a function of hypothetical signal cross section (in pb). Shown are the p -values for the background prediction (dashed black) with regions corresponding to a 1 s.d. and 2 s.d. fluctuation of the backgrounds and the observed data (solid black).

signal with cross section of 4 pb is 8.0×10^{-6} , corresponding to a rejection of this signal cross section at a Gaussian equivalent of 4.3 s.d. We set a 95% C.L. upper limit of 1.9 pb on the production cross section of such a resonance.

In summary, we have used 4.3 fb^{-1} of integrated luminosity collected with the D0 detector to study the dijet invariant mass spectrum in events containing one $W \rightarrow \ell \nu$ ($\ell = e$ or μ) boson decay and two high- p_T jets. Utilizing a similar data selection as the CDF Collaboration we find no evidence for anomalous, resonant

TABLE II: Expected and observed upper limits on the cross section (in pb) at the 95% C.L. for a dijet invariant mass resonance.

M_{jj} (GeV)	110	115	120	125	130	135	140	145	150	155	160	165	170
Expected:	2.20	2.01	1.90	1.78	1.71	1.64	1.58	1.52	1.47	1.40	1.37	1.31	1.24
Observed:	2.57	2.44	2.35	2.27	2.19	2.09	2.00	1.85	1.69	1.58	1.46	1.36	1.28

production of dijets in the mass range 110 – 170 GeV/ c^2 . Using a simulation of $WH \rightarrow \ell\nu b\bar{b}$ production to model acceptance and efficiency, we derive upper limits on the cross section for anomalous resonant dijet production. For $M_{jj} = 145$ GeV/ c^2 , we set a 95% C.L. upper limit of 1.9 pb on the cross section and we reject the hypothesis of a production cross section of 4 pb at the level of 4.3 s.d. In the case that the cross section reported by the CDF Collaboration is modified, we report in Fig. 4 the variation of our p -value for exclusion of potential resonance cross sections other than 4 pb.

We thank the staffs at Fermilab and collaborating institutions, and acknowledge support from the DOE and NSF (USA); CEA and CNRS/IN2P3 (France); FASI, Rosatom and RFBR (Russia); CNPq, FAPERJ, FAPESP and FUNDUNESP (Brazil); DAE and DST (India); Colciencias (Colombia); CONACyT (Mexico); KRF and KOSEF (Korea); CONICET and UBACyT (Argentina); FOM (The Netherlands); STFC and the Royal Society (United Kingdom); MSMT and GACR (Czech Republic); CRC Program and NSERC (Canada); BMBF and DFG (Germany); SFI (Ireland); The Swedish Research Council (Sweden); and CAS and CNSF (China).

- [10] J. Smith, W. L. van Neerven, and J. A. M. Vermaseren, Phys. Rev. Lett. **50**, 1738 (1983).
- [11] T. Sjöstrand, S. Mrenna, and P. Skands, J. High Energy Phys. **05**, 026 (2006). Version 6.3 was used.
- [12] J. Pumplin *et al.*, J. High Energy Phys. **07**, 012 (2002); D. Stump *et al.*, J. High Energy Phys. **10**, 046 (2003).
- [13] M. L. Mangano *et al.*, J. High Energy Phys. **07**, 001 (2003). Version 2.05 was used.
- [14] A. Pukhov *et al.*, arXiv:hep-ph/9908288 (2000).
- [15] R. Brun, F. Carminati, CERN Program Library Long Writeup W5013 (1993).
- [16] N. Kidonakis and R. Vogt, Phys. Rev. D **78**, 074005 (2008).
- [17] N. Kidonakis, Phys. Rev. D **74**, 114012 (2006).
- [18] J. M. Campbell and R. K. Ellis, Phys. Rev. D **60**, 113006 (1999).
- [19] R. Hamberg, W. L. van Neerven, and W. B. Kilgore, Nucl. Phys. B **359**, 343 (1991); B **644**, 403(E) (2002).
- [20] V. M. Abazov *et al.*, Phys. Rev. Lett. **100**, 102002 (2008).
- [21] See Appendix.
- [22] S. Höche *et al.*, arXiv:hep-ph/0602031 (2006).
- [23] W. Fisher, FERMILAB-TM-2386-E (2006).
- [24] T. Junk, Nucl. Instrum. Meth. A **434**, 435 (1999); A. Read, J. Phys. G **28**, 2693 (2002).
- [25] J. Alwall *et al.*, Eur. Phys. C **53**, 473 (2008).

-
- [1] T. Aaltonen *et al.* (CDF Collaboration), Phys. Rev. Lett. **106**, 171801 (2011).
 - [2] D. Acosta *et al.* (CDF Collaboration), Phys. Rev. D **71**, 032001 (2005).
 - [3] V. M. Abazov *et al.* (D0 Collaboration), Phys. Lett. B **698**, 6 (2011).
 - [4] T. Aaltonen *et al.* (CDF Collaboration), Phys. Rev. Lett. **103**, 101802 (2009).
 - [5] V. M. Abazov *et al.* (D0 Collaboration), Phys. Rev. Lett. **102**, 161801 (2009).
 - [6] V. M. Abazov *et al.* (D0 Collaboration), Phys. Rev. Lett. **106**, 171802 (2011).
 - [7] B. Abbott *et al.* (D0 Collaboration), Nucl. Instrum. Methods Phys. Res. A **565**, 463 (2006); M. Abolins *et al.*, Nucl. Instrum. and Methods A **584**, 75 (2007); R. Angstadt *et al.*, Nucl. Instrum. Methods Phys. Res. A **622**, 298 (2010).
 - [8] D0 uses a spherical coordinate system with the z axis running along the proton beam axis. The angles θ and ϕ are the polar and azimuthal angles, respectively. Pseudorapidity is defined as $\eta = -\ln[\tan(\theta/2)]$, in which θ is measured with respect to the proton beam direction.
 - [9] G. C. Blazey *et al.*, arXiv:hep-ex/0005012 (2000). The seeded iterative mid-point cone algorithm with radius $\Delta\mathcal{R} = \sqrt{(\Delta\phi)^2 + (\Delta y)^2} = 0.5$ was used.

APPENDIX

Fit of a 145 GeV/c² Dijet Resonance

The D0 data do not indicate the presence of a non-SM dijet resonance such as indicated by the CDF Collaboration. In the Letter we showed the fit of the SM predictions to the data. However, fitting only the SM contributions could hide an excess if the systematic uncertainties allowed the SM contributions to be distorted in such a way that they filled in the excess. To study this question, we present a fit to the data of the SM predictions plus the Gaussian signal template with $M_{jj} = 145 \text{ GeV}/c^2$. The resulting dijet mass distribution is shown in Fig. 5. The fit is performed in the same way as described in the Letter (no constraint on diboson or W +jets normalizations), except that it now also includes the Gaussian signal template for $M_{jj} = 145 \text{ GeV}/c^2$ with a freely floating normalization. The Gaussian model includes systematic uncertainties affecting both the normalization and shape of the template, analogous to the systematic uncertainties for the diboson prediction. The best fit value for the Gaussian template yields a cross section of $\sigma(p\bar{p} \rightarrow WX) = 0.82^{+0.83}_{-0.82} \text{ pb}$, consistent with no excess. When we fix the diboson cross section to the SM prediction with a Gaussian prior of 7% on the rate, the best fit value for the Gaussian template yields a cross section of $\sigma(p\bar{p} \rightarrow WX) = 0.42^{+0.76}_{-0.42} \text{ pb}$.

Kinematic Corrections to the Simulation

The common tools used to simulate the predicted SM contributions perform well in general, but they have shortcomings. For example, different event generators have different predictions for production angles and relative angles between jets in W +jets and Z +jets events [25]. Thus, it is not unexpected that the simulated W +jets and Z +jets samples do not perfectly model the angular distributions of jets. For analyses with looser selections, such as the search for WH production at D0 [3], these jet angular distributions show clear discrepancies between data and the simulated W +jets and Z +jets events. Thus, these analyses use parameterized functions to correct the pseudorapidities of the two highest p_T jets and the $\Delta\mathcal{R} = \sqrt{(\Delta\eta)^2 + (\Delta\phi)^2}$ separation between those two jets in W/Z +jets samples, and the transverse momentum of the W boson candidate, $p_T(W)$, in the W +jets samples, to better model the data.

The tight kinematic selection criteria employed in this analysis (e.g., $p_T(jj) > 40 \text{ GeV}/c^2$) remove much of the phase space in which the MC generators have difficulty modeling data (e.g., low $p_T(W)$), greatly reducing the need for the kinematic corrections of the simulation. Therefore, the plots and results in the Letter do **not** use any of these kinematic corrections, which is consistent

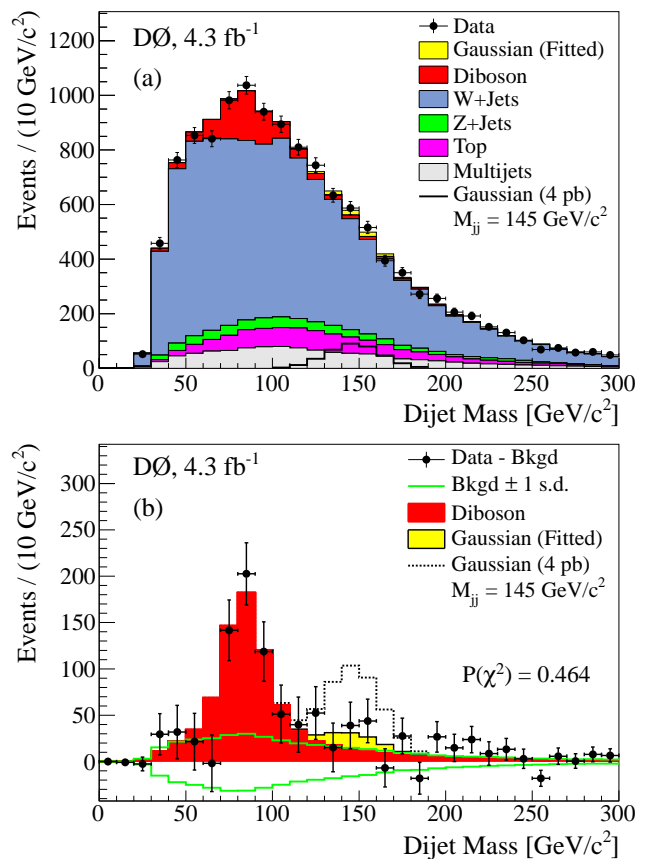


FIG. 5: (color online) Dijet invariant mass summed over lepton channels when including the Gaussian model in the fit to data (a) without and (b) with subtraction of SM contributions other than from the SM diboson processes, along with the ± 1 s.d. systematic uncertainty on all SM predictions.

with the CDF analysis.

Although kinematic corrections are not required to achieve adequate modeling when applying the tight selection criteria of this analysis, modeling issues are probably still present. In this section we present the results obtained when the kinematic corrections (derived from a selection similar to the search for WH production [3]) are applied to this analysis.

The following figures are analogous to those in the Letter, except that the above mentioned kinematic corrections have been applied to the simulation. Figure 6 shows the dijet invariant mass distribution after the fit of the sum of SM predictions to data. The change relative to Fig. 1 in the Letter is not large, but improved modeling is evident in the higher χ^2 probability. The resulting upper limits on the cross section for production of a dijet invariant mass resonance are presented in Table III and shown in Fig. 7. They are consistent with those in Fig. 2 from the Letter. Figure 8 shows the LLR distributions analogous to Fig. 3 from the Letter.

From this study we conclude that the kinematic cor-

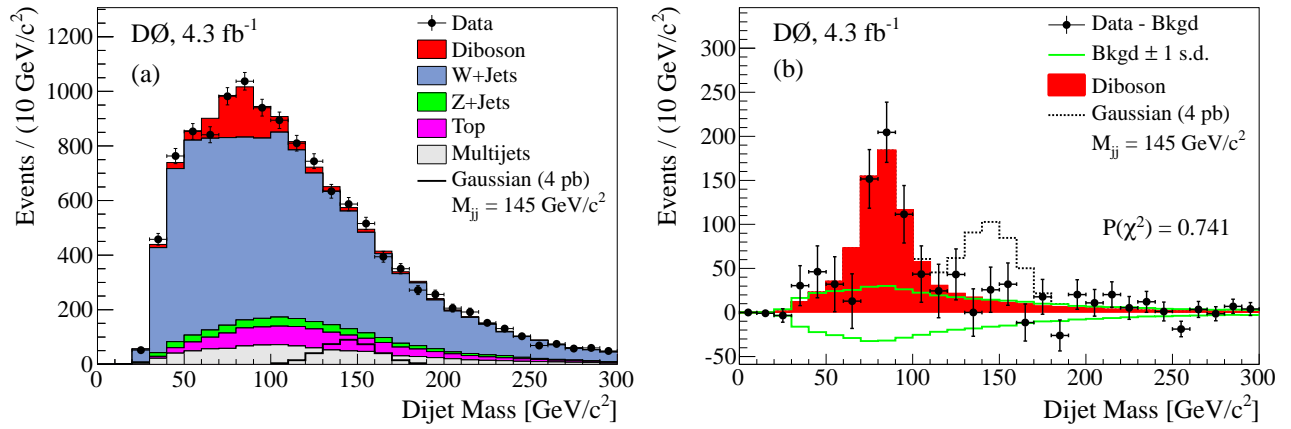


FIG. 6: (color online) Dijet invariant mass summed over lepton channels after the fit (a) without and (b) with SM contributions subtraction other than from the SM diboson processes, along with the ± 1 s.d. systematic uncertainty on all SM predictions. These distributions have the additional kinematic corrections applied to the MC.

TABLE III: Expected and observed upper limits on the cross section (in pb) at the 95% C.L. for a dijet invariant mass resonance. These limits are derived with the additional kinematic corrections applied to the MC.

M_{jj} (GeV)	110	115	120	125	130	135	140	145	150	155	160	165	170
Expected:	2.35	2.16	2.05	1.97	1.88	1.81	1.73	1.68	1.65	1.56	1.52	1.45	1.42
Observed:	2.26	2.02	1.93	1.83	1.74	1.64	1.55	1.48	1.37	1.27	1.18	1.09	1.06

rections to the simulation do not substantially change the result and we reach the same conclusion that there is no excess of dijet events in the D0 data similar to that reported by the CDF collaboration.

Additional Data-MC Comparisons

Kinematic distributions presented in this Section are modeled without the additional corrections applied to the

MC. Figure 9 shows the dijet invariant mass distribution for the separate lepton channels after the simultaneous fit in these two distributions of the SM predictions to data. Figure 1(a) in the Letter is the combination of these two plots. Figure 10 shows comparisons between data and simulation for other kinematic variables after the fit.

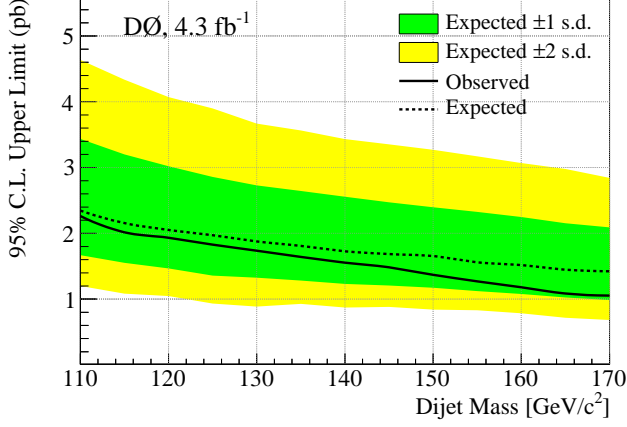


FIG. 7: (color online) Upper limits on the cross section (in pb) at the 95% C.L. for a Gaussian signal in dijet invariant mass. These results are derived with the additional kinematic corrections applied to the MC. Shown in the figure are the limit expected using the background prediction, the observed data limit, and the regions corresponding to a 1 s.d. and 2 s.d. fluctuation of the backgrounds.

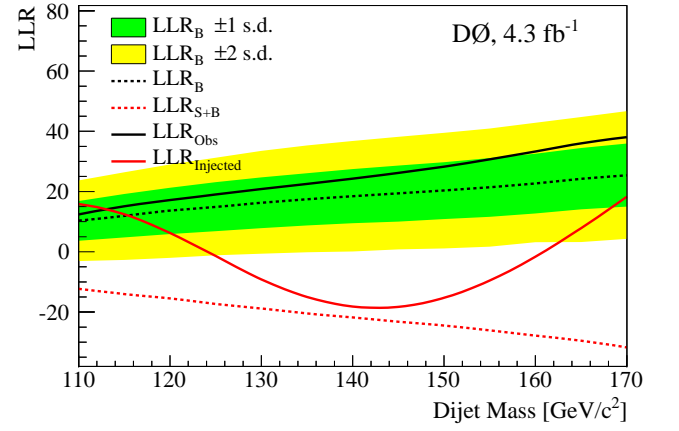


FIG. 8: (color online) Log-likelihood ratio test statistic as a function of probed dijet invariant mass. These results are derived with the additional kinematic corrections applied to the MC. Shown are the expected LLR for the background prediction (dashed black) with regions corresponding to a 1 s.d. and 2 s.d. fluctuation of the backgrounds, for the signal+background prediction (dashed red), for the data (solid black), and for data with a dijet mass resonance at 145 GeV/c^2 injected using a cross section of 4 pb (solid red).

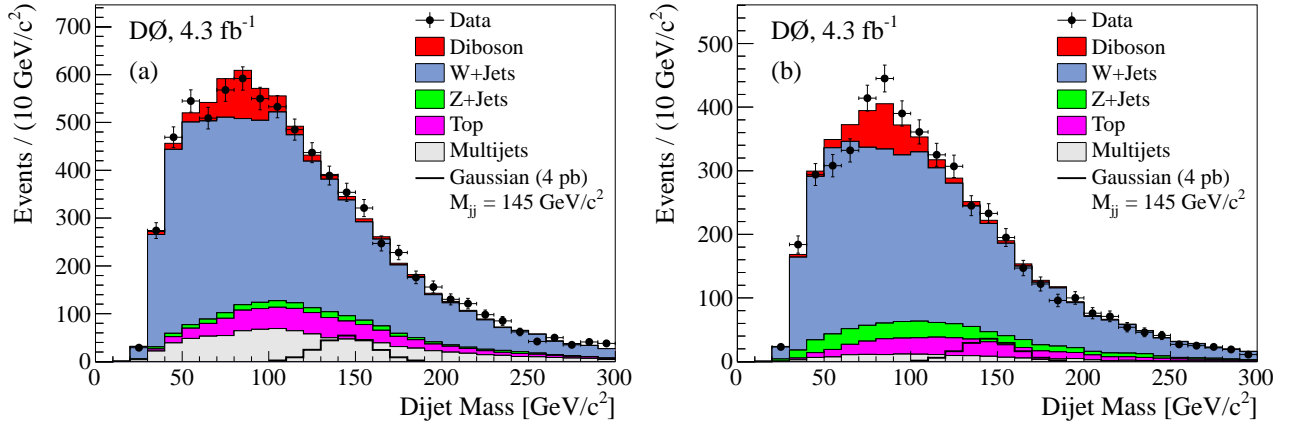


FIG. 9: (color online) Dijet invariant mass distributions separately for the (a) electron and (b) muon channel after the simultaneous fit of these two distributions.

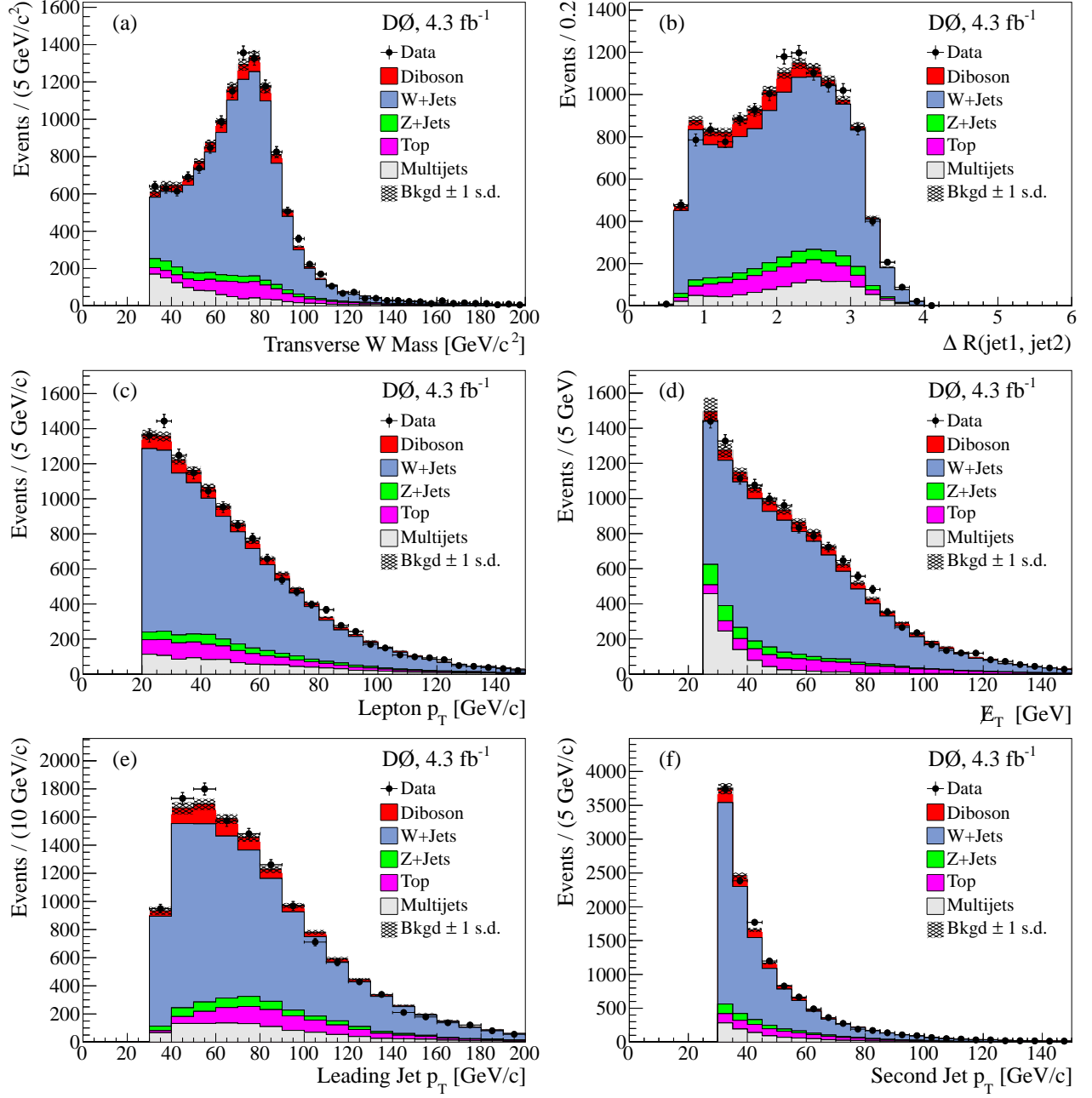


FIG. 10: (color online) Distributions of kinematic variables (combined electron and muon channels) evaluated using the results of a χ^2 fit of SM predictions to data for the dijet invariant mass distribution: (a) transverse W mass, (b) ΔR separation between the two selected jets, (c) lepton p_T , (d) missing transverse energy, (e) highest jet p_T , (f) second highest jet p_T . The ± 1 s.d. systematic uncertainty on all SM predictions is presented by the cross-hatched area.